

UCLA

UCLA Previously Published Works

Title

AGN AND STARBURST IN BRIGHT SEYFERT GALAXIES: FROM IR PHOTOMETRY TO IR SPECTROSCOPY

Permalink

<https://escholarship.org/uc/item/2m72x2jn>

Authors

Spinoglio, L
Tommasin, S
Malkan, MA

Publication Date

2010

Peer reviewed

AGN AND STARBURST IN BRIGHT SEYFERT GALAXIES: FROM IR PHOTOMETRY TO IR SPECTROSCOPY

Luigi Spinoglio,¹ Silvia Tommasin,¹ and Matthew A. Malkan²

RESUMEN

Favor de proporcionar un resumen en español. If you are unable to translate your abstract into Spanish, the editors will do it for you. Infrared photometry and later infrared spectroscopy provided powerful diagnostics to distinguish between the main emission mechanisms in galaxies: AGN and Starburst. After the pioneering work on infrared photometry with *IRAS* in the far-IR and the S.Pedro Martir and ESO ground-based work in the near-IR, ISO photometry extended up to $200\mu\text{m}$ the coverage of the galaxies energy distributions. Then *Spitzer* collected accurate mid-infrared spectroscopy on different samples of galaxies. We will review the work done on the $12\mu\text{m}$ galaxy sample since the times of *IRAS* photometry to the new *Spitzer* spectroscopy. The main results on the multifrequency data of $12\mu\text{m}$ selected Seyfert galaxies are presented and discussed in the light of unification and evolution models. The spectroscopic work of *Spitzer* will soon be complemented at longer wavelengths by the *Herschel* spectrometers and in the future by *SPICA* at higher redshift.

ABSTRACT

Infrared photometry and later infrared spectroscopy provided powerful diagnostics to distinguish between the main emission mechanisms in galaxies: AGN and Starburst. After the pioneering work on infrared photometry with *IRAS* in the far-IR and the S.Pedro Martir and ESO ground-based work in the near-IR, ISO photometry extended up to $200\mu\text{m}$ the coverage of the galaxies energy distributions. Then *Spitzer* collected accurate mid-infrared spectroscopy on different samples of galaxies. We will review the work done on the $12\mu\text{m}$ galaxy sample since the times of *IRAS* photometry to the new *Spitzer* spectroscopy. The main results on the multifrequency data of $12\mu\text{m}$ selected Seyfert galaxies are presented and discussed in the light of unification and evolution models. The spectroscopic work of *Spitzer* will soon be complemented at longer wavelengths by the *Herschel* spectrometers and in the future by *SPICA* at higher redshift.

Key Words: Galaxies: Active — Galaxies: Starbursts — Infrared: Galaxies

1. INTRODUCTION

The interrelationship between *star formation* and *accretion* onto massive black holes is crucial to understanding galaxy formation and evolution. On a cosmic scale, the evolution of supermassive black holes appears tied to the evolution of the star-formation rate (Marconi et al 2004; Merloni et al 2004). The growth of bulges through *star formation* may be directly linked to the growth of black holes through accretion (Heckman et al 2004). On a local scale, evidence is mounting that *star formation* and nuclear activity are linked. Two possible evolutionary progressions can be predicted: HII/Starburst galaxies \rightarrow Seyfert 2 (Storchi-Bergmann et al 2001;

Kauffmann et al 2003), or a fuller scenario of HII/Starburst galaxies \rightarrow Seyfert 2 \rightarrow Seyfert 1 (Hunt & Malkan 1999; Levenson et al 2001; Krongold et al 2002). These predict that galaxy interactions, leading to the concentration of a large gas mass in the circumnuclear region of a galaxy, trigger starburst emission. Then mergers and bar-induced inflows can bring fuel to a central black hole, stimulating AGN activity. While relatively young (~ 1 Gyr) stellar populations are found in more than half of Seyfert 2s (Schmitt et al 1999; González Delgado et al 2001; Raimann et al 2003), they are also found in broad-lined AGNs (Kauffmann et al 2003). However, any firm conclusion cannot rely on optical spectra of optically selected samples of galaxies. Photometric mid-IR studies (Edelson Malkan & Rieke 1987; Maiolino et al 1995) did indeed find that Seyfert 2s galaxies more often have enhanced star formation than Seyfert 1s and the near and far-IR observations

¹Istituto di Fisica dello Spazio Interplanetario, INAF, Via Fosso del Cavaliere 100, I-00133, Roma, Italy (luigi.spinoglio, silvia.tommasin@ifsi-roma.inaf.it).

²Astronomy Division, University of California, Los Angeles, CA 90095-1547, USA (malkan@astro.ucla.edu).

of the $12\mu\text{m}$ galaxy sample (Spinoglio et al 1995) show systematic differences between type 1's and type 2's spectral energy distributions. However, detailed *infrared spectroscopy* is necessary to better separate the star formation and accretion components in the energy budget of active galaxies and strengthen the hypothesis of an evolutionary difference between different types of active galaxies. Better understanding the *star formation* versus *accretion* connection requires mid-infrared spectroscopy of representative samples of active galaxies in the local universe. This is because active galactic nuclei (AGNs) are often very dusty, locally and even at high redshifts (Priddey et al 2003; Bertoldi et al 2003). Similarly, *star formation* activity, which often coexists with AGN activity, is also heavily enshrouded in dust.

We review in this article the great amount of observational work that has been done on the $12\mu\text{m}$ galaxy sample and in particular on its subsample of active galaxies.

2. THE $12\mu\text{M}$ ACTIVE GALAXIES SAMPLE

The sample that is less biased and most representative of the local active galaxies populations is selected from the $12\mu\text{m}$ Galaxy Sample (12MGS), an IRAS-selected all-sky survey flux-limited to 0.22 Jy at $12\mu\text{m}$ (Rush, Malkan & Spinoglio 1993, hereafter RMS) and form the complete sub-samples of Seyfert 1s and Seyfert 2s of the entire 12MGS. This is essentially a bolometric flux-limited survey outside the galactic plane, because of the empirical fact that all *galaxies* emit a constant fraction of their total bolometric luminosity at $12\mu\text{m}$. This fraction is $\sim 9\text{-}13\%$ for AGNs and $\sim 7\text{-}8\%$ for normal and starburst galaxies, independent of

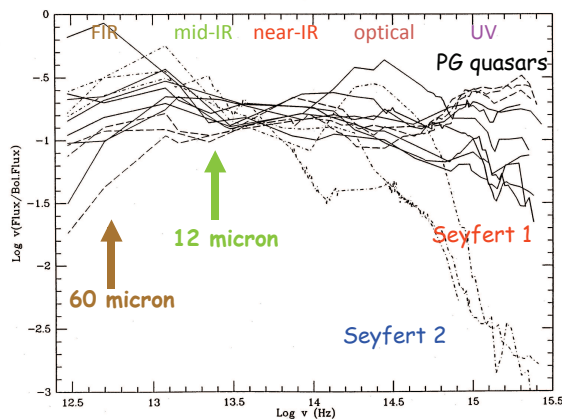


Fig. 1. Spectral energy distributions of 13 AGN normalized to the bolometric fluxes (Spinoglio & Malkan 1989).

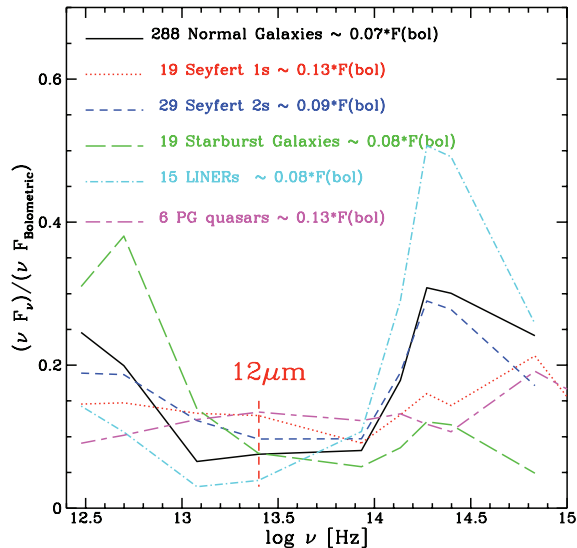


Fig. 2. Average SEDs of the various types of galaxies normalized to their bolometric fluxes (Spinoglio et al 1995).

star formation activity (Spinoglio et al 1995). For Seyfert galaxies and quasars, this can be seen in Figure 1, which shows the spectral energy distributions of 13 active galaxies normalized to their bolometric flux: the minimum scatter among the different types of galaxies appears in the range $7\text{-}12\mu\text{m}$ (Spinoglio & Malkan 1989). For the different types of $12\mu\text{m}$ selected galaxies, normal, Seyfert, starburst galaxies and LINERs, compared to a small sample of PG quasars, the spectral energy distributions normalized to their bolometric fluxes are shown in Figure 2. Finally, the 12MGS is less subject to contamination by high star-formation rate objects than other infrared samples defined at longer wavelengths (Hunt & Malkan 1999).

$12\mu\text{m}$ selection finds obscured objects via re-radiation of their primary emission by dust. An alternative way of finding obscured AGN is by selecting directly on their accretion radiation at hard X-rays, insensitive to all but the heaviest intrinsic absorption. However, unlike the 12MGS, as shows Figure 3, the hard X-ray selected samples miss most of the Compton thick objects ($N_{\text{H}} > 10^{24} \text{ cm}^{-2}$).

The 12MGS contains 53 Seyfert 1s and 63 Seyfert 2s (RMS). This sample has a complete set of observations at virtually every wavelength: full IRAS and near-IR coverage (RMS; Spinoglio et al 1995), X rays (Rush et al 1996), optical spectroscopy, radio (Rush Malkan & Edelson 1996), optical/IR imaging (Hunt & Malkan 1999; Hunt et al 1999), $100\text{-}200\mu\text{m}$ far-infrared photometry from ISOPHOT

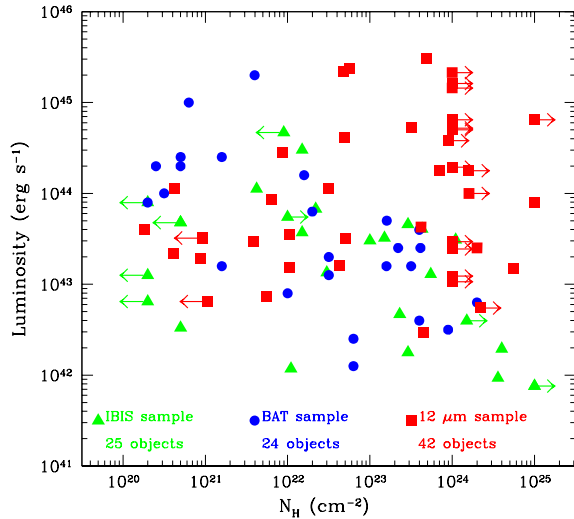


Fig. 3. Luminosity-Hydrogen absorption column density *plane* of the $12\mu\text{m}$ Seyfert (squares) detected at hard X-rays. Hard-X-ray selected AGNs, from IBIS (triangles) and Bat (circles), are shown for comparison.

(Spinoglio Andreani & Malkan 2002). In the recent years $10\mu\text{m}$ imaging (Gorjian et al. 2004), $2.8\text{--}4.1\mu\text{m}$ slit spectroscopy (Imanishi 2003; Imanishi & Alonso-Herrero 2004) optical spectropolarimetry (Tran 2001; Tran 2003) radio observations (Thean et al 2000; Thean et al 2001) and *Spitzer* low resolution spectra (Buchanan et al 2006) have been collected for most of the Seyfert galaxies in our sample. Finally a first article on the high resolution *Spitzer* spectra has been published (Tommasin et al 2008) and another one is completing the mid-infrared spectral coverage of almost all the sample (Tommasin et al 2009).

2.1. The $12\mu\text{m}$ and the line luminosity functions of Seyfert galaxies

The $12\mu\text{m}$ luminosity function of the Seyfert galaxies of the 12MGS has been derived by RMS. There is no significant difference between the two types of Seyfert, as one can see from Figure 4, except for the fact that at the highest luminosities ($L > 10^{12}L_{\odot}$) only type 1's are found. We note, however, that this can be due to the inclusion in this latter class of the few blazars and quasars present in the 12MGS.

The analysis of the optical and ultraviolet emission line spectra has been done recently (Rodriguez et al 2009). The luminosity functions of all the narrow lines for which there is enough statistics ($[\text{OI}]\lambda 6300\text{\AA}$, $[\text{OII}]\lambda 3727\text{\AA}$, $[\text{OIII}]\lambda 4959\text{\AA}$, $[\text{OIII}]\lambda 5007\text{\AA}$, $[\text{NII}]\lambda 6584\text{\AA}$ and

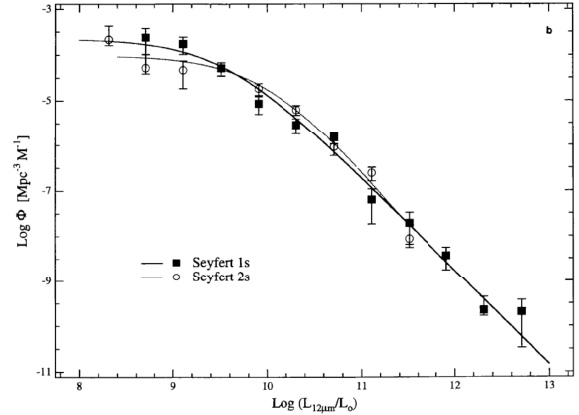


Fig. 4. The $12\mu\text{m}$ luminosity function of Seyfert galaxies (RMS).

$[\text{SII}]\lambda\lambda 6717+6734\text{\AA}$) are the same for both types of Seyfert's. Only the $\text{H}\alpha$ and $\text{H}\beta$ luminosity functions show more Seyfert 1's at high luminosities compared to Seyfert 2's. This difference can be understood because type 1's have substantial emission in both these lines from their Broad Line Regions. The luminosity functions for $\text{H}\alpha$, $\text{H}\beta$, $[\text{OIII}]\lambda 5007\text{\AA}$ and $[\text{OII}]\lambda 3727\text{\AA}$ are displayed in Figure 5.

The agreement between the $12\mu\text{m}$ continuum and the narrow lines luminosity functions testifies that these quantities are all isotropic and are not affected by the geometry or disk/torus orientation. This also implies that the $12\mu\text{m}$ selection is not biased against or in favor of Seyfert types 1 or types 2.

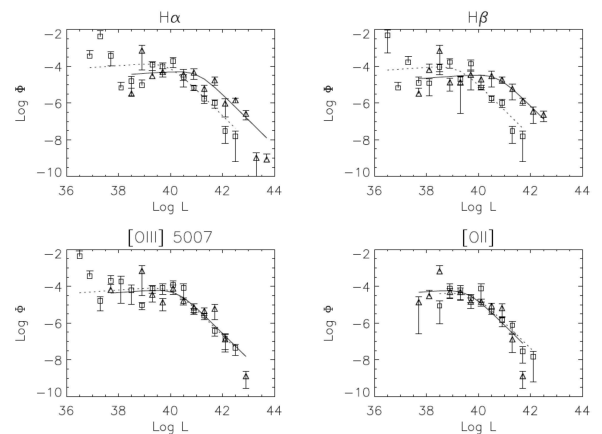


Fig. 5. Emission line luminosity functions for $\text{H}\alpha$, $\text{H}\beta$, $[\text{OIII}]\lambda 5007\text{\AA}$ and $[\text{OII}]\lambda 3727\text{\AA}$ for the $12\mu\text{m}$ selected Seyfert galaxies (Rodriguez et al 2009). Triangles represent Seyfert 1's and squares Seyfert 2's.

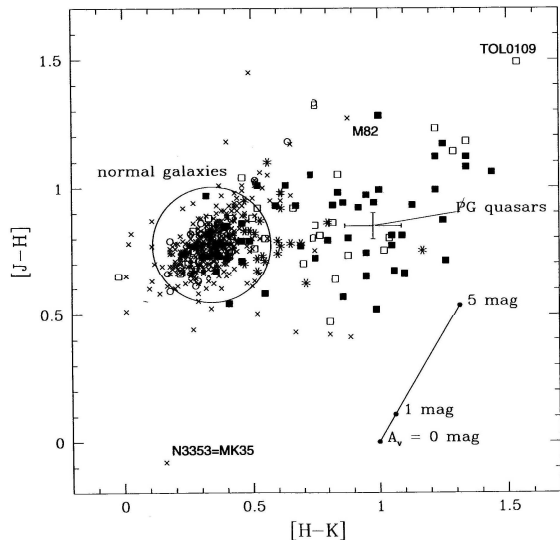


Fig. 6. $[J - H]$ vs. $[H - K]$ diagram with Seyfert 1's (*filled squares*), Seyfert 2's (*open squares*), Normal's (*crosses*) (Spinoglio et al 1995).

3. INFRARED PHOTOMETRY

3.1. Total near-infrared fluxes

Infrared photometry has been used to isolate star formation and accretion processes. A large observational effort has been done to observe in the J, H, K and, in some cases, L bands as many as 321 galaxies from the $12\mu\text{m}$ galaxy sample (Spinoglio et al 1995).

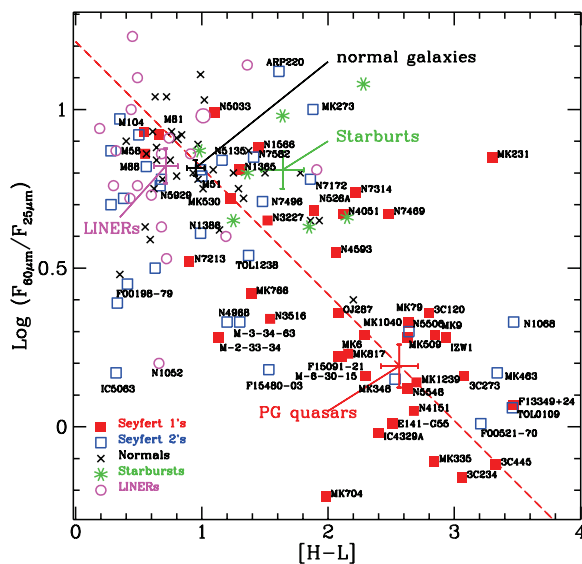


Fig. 7. Composite near-far-IR color-color diagram: the $[H - L]$ color versus the $60\mu\text{m}/25\mu\text{m}$ flux ratio (Spinoglio et al 1995).

At the 2.1m telescope of the S. Pedro Martir Observatory, thanks to a collaboration with Luis Carrasco and Elsa Recillas, we observed the northern galaxies, while those of the southern hemisphere were observed at the 1m ESO telescope (La Silla, Chile).

To be able to compare the large beam IRAS data (RMS) with the near-IR data, derive spectral energy distributions and build meaningful color-color diagrams, we have computed the near-IR total fluxes using growth curves (Spinoglio et al 1995). Combining the IRAS and near-IR data we were able to derive the spectral energy distributions (SED) of hundreds of galaxies. As presented in the previous section, we show in Figure 2 the average SEDs, normalized to their bolometric flux, of normal, Seyfert and starburst galaxies, as well as LINERs and PG quasars.

We have found that color-color diagrams are very effective in separating the different galaxy types. The usual $[J - H]$ versus $[H - K]$ color-color diagram shown in Figure 6 can separate many Seyfert galaxies from normal galaxies: at $2.2\mu\text{m}$ the strong thermal emission from hot dust grains illuminated by the active nucleus rises above starlight from red giants, peaking in the H photometric band and dominating the stellar component in galaxies.

In Figure 7 we show the $[H - L]$ color versus the $60\mu\text{m}/25\mu\text{m}$ flux ratio. This plot can separate nor-

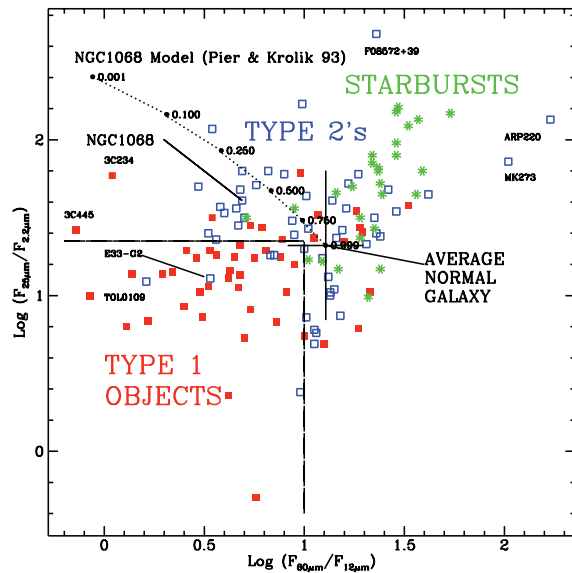


Fig. 8. Color-color diagram separating Seyfert 1's, 2's and starburst galaxies. The dotted line shows a mixture of the NGC1068 torus model colors (Pier & Krolik 1993) and the average galactic colors. The symbols are the same as in the previous figure (Spinoglio et al 1995).

mal and starburst galaxies from Seyfert type 1 and PG quasars, because the former have steep far-IR slopes and bluer near-IR spectra, while the latter have flatter far-IR SEDs and redder near-IR slopes. As most Seyfert 1's are located at the lower right part of the diagram, while most type 2's lie in the upper left corner, where only a few Seyfert 1's are found (most of which are nearby Messier galaxies) demonstrate that the SEDs of the two Seyfert populations are indeed different.

In Figure 8 we show the $60\mu\text{m}/12\mu\text{m}$ versus the $25\mu\text{m}/2.2\mu\text{m}$, as suggested previously for an analysis of the CfA Seyfert galaxies (Edelson Malkan & Rieke 1987), where it is clear a segregation of the Seyfert type 1's in the lower left part of the diagram, at the flatter spectral slopes: 30/48 type 1s and only 5/52 type 2s occupy this region. The presence of an optically thick edge-on torus (Pier & Krolik 1993) would indeed steepen the SED by absorbing high energy radiation and re-emitting it at longer wavelengths.

3.2. Bolometric luminosities of Seyfert and normal galaxies

Spinoglio et al (1995) determined for the first time the bolometric luminosities of a large sample of galaxies, both Seyfert and normal galaxies. One of their most important result is the linear relation found between the $12\mu\text{m}$ and *bolometric* luminosities for both Seyfert and normal galaxies.

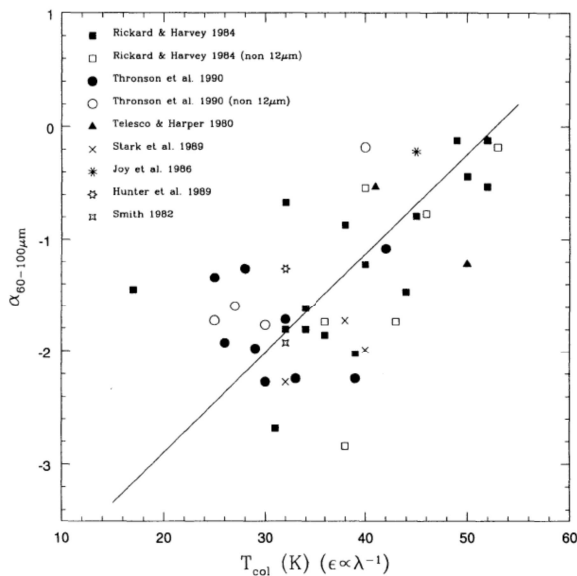


Fig. 9. Least squares fit of the spectral index $\alpha_{60-100\mu\text{m}}$ as a function of the color temperature, assuming graybody emission (Spinoglio et al 1995).

To obtain reliable *bolometric luminosities* for the galaxies, we have used the IRAS $[60-100\mu\text{m}]$ color to predict the far-IR turnover. Figure 9 shows the correlation between color temperature and IRAS spectral index. From the fit shown, we derived the relation:

$$T_{color} = 11.4 \times (\alpha_{60-100\mu\text{m}} + 4.67)K$$

We then computed the submillimeter fluxes beyond $100\mu\text{m}$ assuming a graybody at the derived color temperature, with a dust emissivity $\epsilon \propto \lambda^{-1}$.

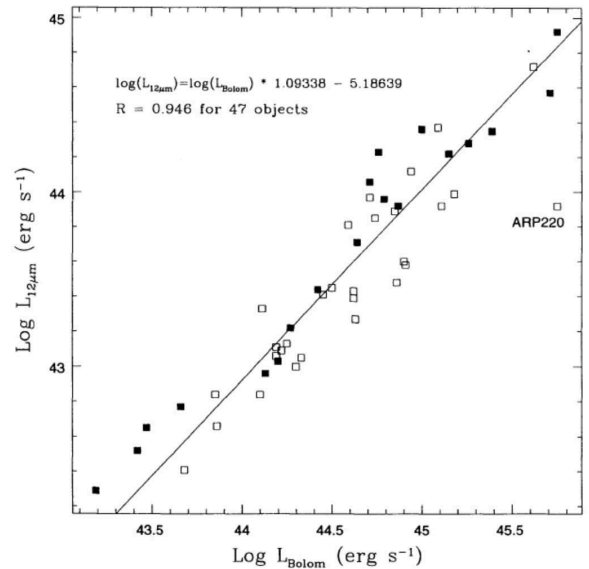


Fig. 10. $12\mu\text{m}$ vs bolometric luminosity for Seyfert 1's (filled squares) and 2's (open squares). The line represents the least squares fit to all data, except Arp220 (Spinoglio et al 1995).

For the Seyfert galaxies, the relation between the $12\mu\text{m}$ and the bolometric luminosity is shown in Figure 10, with a slope of 1.09 (with a regression coefficient of $R=0.95$). We notice that a similar relation between bolometric luminosity and the other IRAS bands monochromatic luminosities is poorer compared to the $12\mu\text{m}$ band: at $25\mu\text{m}$ the slope is 1.19 ($R=0.90$), at $60\mu\text{m}$ the slope is 1.19 ($R=0.91$) and at $100\mu\text{m}$ the slope is 1.13 (with a poorer $R=0.93$).

For the normal galaxies, the relation between the $12\mu\text{m}$ and the bolometric luminosity is shown in Figure 11, with a slope of 1.06 (with a regression coefficient of $R=0.94$). A similar relation between bolometric luminosity and the other IRAS bands monochromatic luminosities is poorer compared to the $12\mu\text{m}$ band: at $25\mu\text{m}$ the slope is 1.15 ($R=0.93$), at $60\mu\text{m}$ the slope is 1.12 ($R=0.94$) and at $100\mu\text{m}$ the slope is 1.11 (with a poorer $R=0.89$).

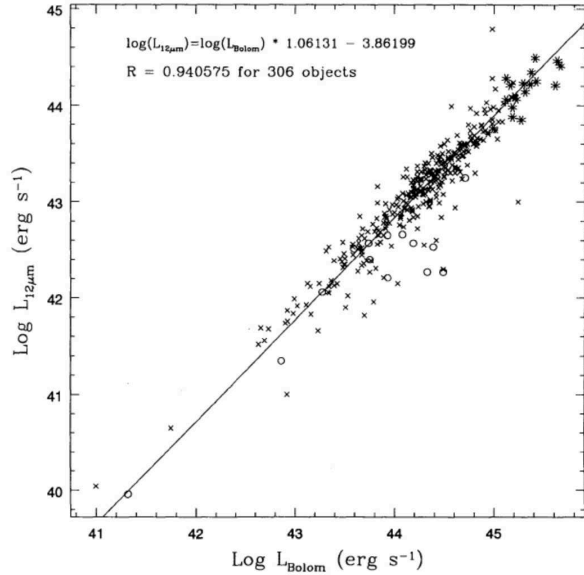


Fig. 11. $12\mu\text{m}$ vs bolometric luminosity for normal galaxies (*crosses*), starburst's (*asterisks*) and LINERs (*open circles*). The line represents the least squares fit to all data (Spinoglio et al 1995).

3.3. Extending to $200\mu\text{m}$ with ISO

With the launch of the *Infrared Space Observatory*, we were able to collect far-infrared photometry between 100 and $200\mu\text{m}$ for the $12\mu\text{m}$ galaxies (Spinoglio Andreani & Malkan 2002). We have fol-

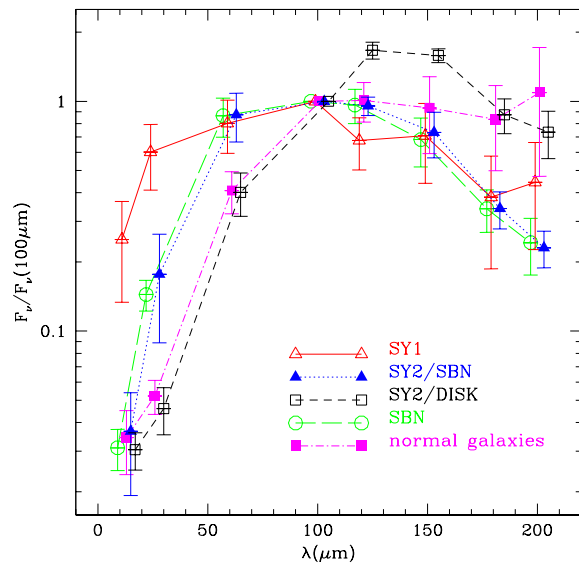


Fig. 12. The average spectral energy distributions of Seyfert, starbursts and normal galaxies, normalized to the $100\mu\text{m}$ flux (Spinoglio Andreani & Malkan 2002).

lowed Rowan-Robinson & Crawford (1989) in using the 12-25-60- $100\mu\text{m}$ colors to identify those galaxies in our sample that closely resemble the SEDs of the *quiescent cirrus* disk, the starburst component, and the *pure Seyfert* nucleus. For each of the three types of galaxies - the normal spirals, the starburst galaxies, and the Seyfert 1's - we have selected those objects lying in the two IRAS color-color diagrams close (i.e., within 0.2 mag) to the colors of *pure disk*, *starburst*, and *Seyfert* components (Rowan-Robinson & Crawford 1989). We have plotted in Figure 12 the average $12\text{-}200\mu\text{m}$ SEDs for each class. A strong distinction is apparent out to $200\mu\text{m}$ between the quiescent disk component and the starburst component. These components represent the extremes of minimal and maximal recent star formation found in the least and most luminous galaxies, respectively. The pure Seyfert spectrum is rather similar to the pure starburst spectrum between 100 and $200\mu\text{m}$. Both show a relative lack of cold dust, and the Seyferts spectra tend to be weaker at $120\mu\text{m}$.

The Seyfert 2's are spread all around the IRAS color-color diagrams. As can be seen in Figure 12, some of them (SY2/SBN) have IRAS spectra close to the pure starburst template. And indeed, their ISOPHOT far-infrared spectra also match the pure starburst spectrum well, since their infrared continuum appears to be dominated from dust around star-forming regions. Those Seyfert 2's with IRAS colors

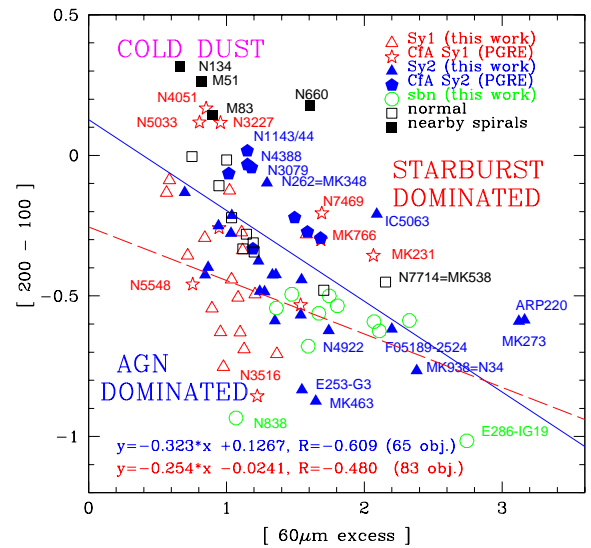


Fig. 13. $[200 - 100\mu\text{m}]$ color vs. the $60\mu\text{m}$ excess diagram of galaxies belonging to the $12\mu\text{m}$ galaxy sample (Spinoglio Andreani & Malkan 2002).

like quiescent cirrus disks (SY2/DISK) also resemble pure disks in the 100-200 μm region. Again, it appears that the Seyfert 2 nucleus contributes a minor fraction of the observed far-infrared luminosity in those objects.

We have chosen as the indicator of enhanced recent star formation, which warms dust around HII regions, the 60 μm *excess* as the ratio of the observed 60 μm flux to the flux that a source would have at 60 μm from power-law interpolation of the flux between 12 and 100 μm . Figure 13 shows the [200 - 100 μm] color versus the 60 μm *excess*.

While this diagram does not separate the galaxies of different classes perfectly, it nevertheless shows that they cluster preferentially in different regions of the diagram. Seyfert 1's (excluding six objects of the CfA sample) cluster in a no 60 μm excess region with a color [200 - 100 μm] < 0. The starburst galaxies cluster in the central area of the diagram and have all 60 μm excess. Normal galaxies and nearby spirals have no 60 μm excess (except two objects) and a [200 - 100 μm] color between -0.5 and +0.5. Seyfert 2's are widely spread all over the diagram, but with a 60 μm excess generally higher than Seyfert 1's.

We suggest that the diagram shown in Figure 13 can be used to separate the starburst-dominated objects from the AGN-dominated ones. Objects located in the upper right part of the diagram are likely *starburst-dominated*, while those at the left, having a fainter excess, are the *AGN-dominated* objects. We suggest that starburst activity in galaxies, i.e., with high rates of current star formation, results in excess emission in the 60 μm band accompanied by a general heating of the galactic interstellar medium and thus a decrease of the [200 - 100 μm] color.

4. INFRARED SPECTROSCOPY

Mid-IR and far-IR spectroscopy of fine-structure emission lines are powerful tools to understand the physical conditions in galaxies.

Figure 14 shows the critical density (i.e. the density for which the rates of collisional and radiative de-excitation are equal) of a line versus the ionization potential of its ionic species. It shows how these lines can measure density and ionization of the gas: the ratio of lines with similar critical density, but different ionization potential, measures the ionization, while the ratio of lines with similar ionization potential, but different critical density, measures the density (Spinoglio & Malkan 1992). Lines from different emission regions in galaxies are shown with different symbols. Infrared spectroscopy has a thorough diagnostic power for gas with densities from

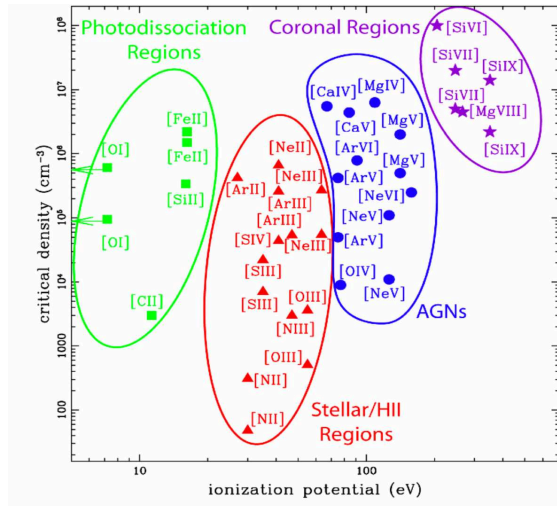


Fig. 14. The power of the infrared fine-structure lines to trace the different physical regimes: *From left to right*: low-ionization/photodissociation regions, stellar/HII regions, AGN emission line regions, Coronal line regions (Spinoglio & Malkan 1992).

10^2 cm^{-3} to 10^8 cm^{-3} and ionization potentials up to 350 eV, using the so called coronal lines. Moreover, increasing its wavelength, an IR spectral line becomes more insensitive to dust extinction, and can therefore probe regions highly obscured at optical or even near-to-mid infrared wavelengths.

Besides the ionic fine-structure lines, the mid-IR spectrum of galaxies also contains strong features due to the emission of Polycyclic Aromatic Hydrocarbons (Puget & Leger 1989), hereafter PAH. These features have been observed in ultraluminous IR galaxies with the *ISO* SWS spectrometer (Genzel et al 1998). They are present while star formation is active and disappear when illuminated by the strong ionizing field of active nuclei.

4.1. Far-IR spectroscopy with ISO-LWS

Far-infrared spectroscopy has been so far collected by the LWS spectrometer onboard of *ISO* (Kessler et al 1996) only on a few bright active and ultraluminous IR galaxies, showing an unexpected sequence of features from strong [OIII]52, 88 μm and [NIII]57 μm line emission to detection of only faint [CII]157 μm line emission and [OI]63 μm in absorption, and molecular lines almost always in absorption (Fischer et al 1999). A few studies have been dedicated to individual galaxies, e.g. M82 (Colbert et al 1999), Arp220 (González-Alfonso et al 2004),

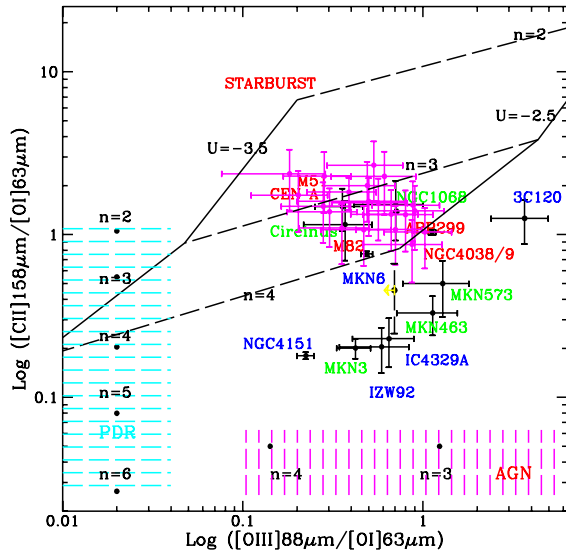


Fig. 15. ISO-LWS line ratio diagram (Spinoglio et al 2003). Seyfert 1's: blue, Seyfert 2's: green, starburst galaxies: red. Pink crosses: nearby galaxies (Negishi et al 2001). Grid: starburst models with different densities and ionization parameter. Vertical hatched area: the $[CII]/[OI]$ ratio for PDR models ($\log n=2-6 \text{ cm}^{-3}$, $\log G_0=3$). Horizontal hatched area: the $[OIII]/[OI]$ ratio for AGN models ($\log U=-2.5$, $\log n=3, 4 \text{ cm}^{-3}$).

NGC1068 (Spinoglio et al 2005), Mrk231 (González-Alfonso et al 2008). A systematic far-infrared spectroscopic survey of Seyfert and ULIRGs will have to wait for the *Herschel* mission. However the few data available already revealed the diagnostic power of the FIR fine structure lines. Figure 15 (Spinoglio et al 2003) shows the $[CII]158\mu\text{m}/[OI]63\mu\text{m}$ ratio versus the $[OIII]88\mu\text{m}/[OI]63\mu\text{m}$ ratio. Normal galaxies cluster together with the Seyfert's having strong starburst emission (e.g. NGC1068) and coincide with predicted ratios for typical starburst galaxies. However, at lower values of the $[CII]/[OI]$ ratio, most of the AGN are clustering in a strip with higher ratio of $[OI]/[CII]$ compared to starburst galaxies. This may arise from X-Ray Dissociation Regions (XDRs), whose $[OI]/[CII]$ ratios are larger than in PDRs. Thus the 3 strongest FIR emission lines can separate the 3 basic energy sources in galaxies: a) the AGN produces strongly emission from highly ionized gas, with $[OIII]$ being prominent in the NLR, but also unusually strong $[OI]63\mu\text{m}$ because this neutral line is strong in XDRs (Meijerink et al 2007), and has a very high critical density ($\sim 10^6 \text{ cm}^{-3}$). All

the classical Seyfert galaxies in Figure 15 lie in the bottom part of the diagram, below any of the starburst models. b) recent star formation, which produces $[OIII]$ in the high-excitation HII regions, as well as strong $[CII]158\mu\text{m}$ in the PDRs which tend to surround these star forming regions; and c) pure PDR emission from the quiescent disk of the spiral galaxy, which produces strong $[CII]$ and $[OI]$ emission, but no $[OIII]$. The most quiescent spirals lie in the upper left side of the diagram (Negishi et al 2001).

4.2. Mid-IR spectroscopy with Spitzer

In the very rich mid-infrared spectra of active galaxies we can identify various indicators of AGN dominance, e.g. the line ratios of $[NeV]/[NeII]$, $[NeV]/[SiII]$, $[OIV]/[NeII]$, as well as indicators of star formation dominance, e.g. the PAH emission bands, the H_2 rotational lines and nebular emission lines mainly originated in HII regions, e.g. from $[SIII]$ and $[NeII]$.

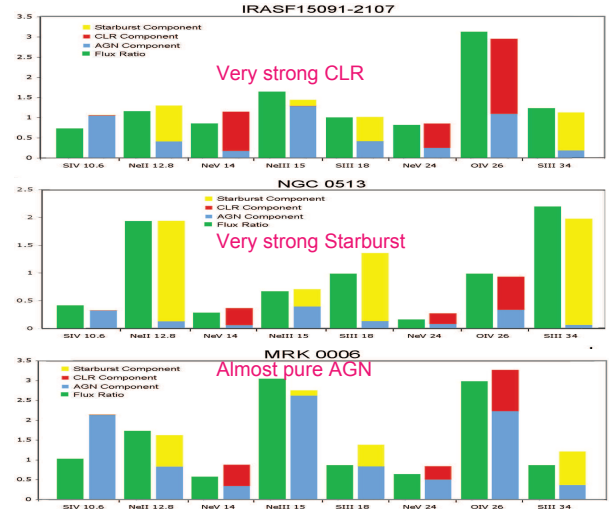


Fig. 16. Comparison of the observed and modelled spectra for three sample Seyfert galaxies: (Hainline et al. 2009).

The diagnostic power of the mid-IR fine structure lines can be quantified from the decomposition of the observed spectra in terms of three different photoionized components (Hainline et al. 2009): (a) *AGN model*: with metallicity Z solar, spectral slope $\alpha=-1.7$, density $n=10^3$, and ionization potential: $\log U = -2$ (Groves et al 2004); (b) *Starburst model*: with metallicity $Z = 2 \times Z_{\odot}$, age range = $0.1 - 6 \text{ Myr}$, $\log R = (M_{cl}/M_{\odot})/(Po/k) = -6$, (Dopita et al 2006); (c) *a Coronal line region model (CLR)*: $\log U = 0$ at the inner radius of the region and

spectral slope $\alpha = -1.0$ (Spinoglio & Malkan 1992). Figure 16 shows such a decomposition for the mid-IR spectra of three sample objects: IRASF15091-2107 for which a strong CLR is present, NGC513 for which a strong Starburst component is necessary to fit the data and Mrk6, which is almost a "pure" AGN.

The first results of the *Spitzer* spectroscopic survey of the Seyfert galaxies of the $12\mu\text{m}$ sample (Tommasin et al 2008) show a clear inverse trend between the indicator of *AGN dominance*, the $[\text{NeV}]14.3\mu\text{m}/[\text{NeII}]12.8\mu\text{m}$ line ratio, and the equivalent width of the $11.25\mu\text{m}$ PAH feature, which can be considered as an indicator of the *star formation dominance*, as shown in Figure 17. Here the Seyfert galaxies have been reclassified, following the results of spectropolarimetry (author?) (Tran 2001, Tran 2003), in type 1's (including the classical Seyfert 1's and the hidden Broad Line Region Seyfert 2's, as discovered through spectropolarimetry) and "pure" type 2's (for which a BLR was not detected). Most of the type 1 objects, including both Seyfert 1s and hidden Broad Line Region Seyfert 2s, are located at high values of the $[\text{NeV}]14.3\mu\text{m}/[\text{NeII}]12.8\mu\text{m}$ line ratio and very low or absent PAH emission.

Another diagnostic diagram using both spectroscopic and photometric results is shown in Figure 18: the spectral index between 25 and $60\mu\text{m}$ $\alpha_{(60\mu\text{m}-25\mu\text{m})}$ versus the $[\text{NeV}]14.3\mu\text{m}/[\text{NeII}]12.8\mu\text{m}$ line ratio. A clear trend shows that when the *AGN*

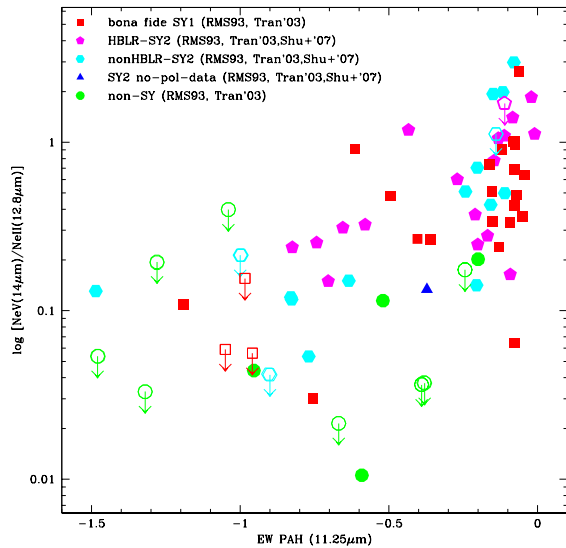


Fig. 17. $[\text{NeV}]14.3\mu\text{m}/[\text{NeII}]12.8\mu\text{m}$ line ratio versus the equivalent width of the $11.25\mu\text{m}$ PAH. (Tommasin et al 2008; Tommasin et al 2009).

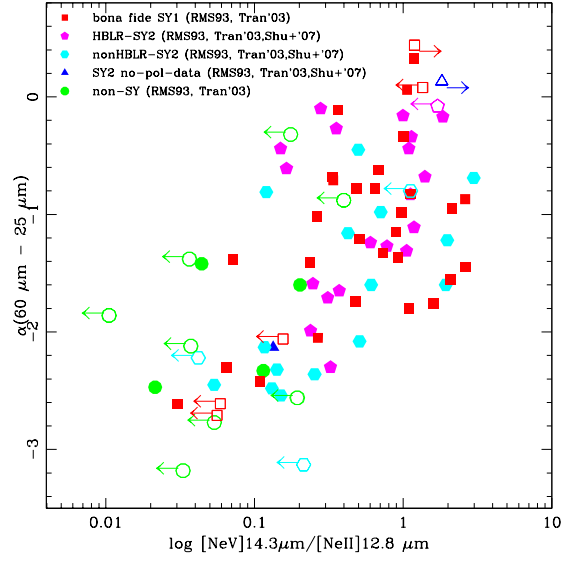


Fig. 18. The mid-to-far-IR spectral index $\alpha_{(60\mu\text{m}-25\mu\text{m})}$ versus the $[\text{NeV}]14.3\mu\text{m}/[\text{NeII}]12.8\mu\text{m}$ line ratio. (Tommasin et al 2008).

dominance increases, the spectral index flattens. Most of type 1 objects appear to be concentrated in the upper right part of the diagram, at high values of *AGN dominance* and flat mid-to-far-IR slopes.

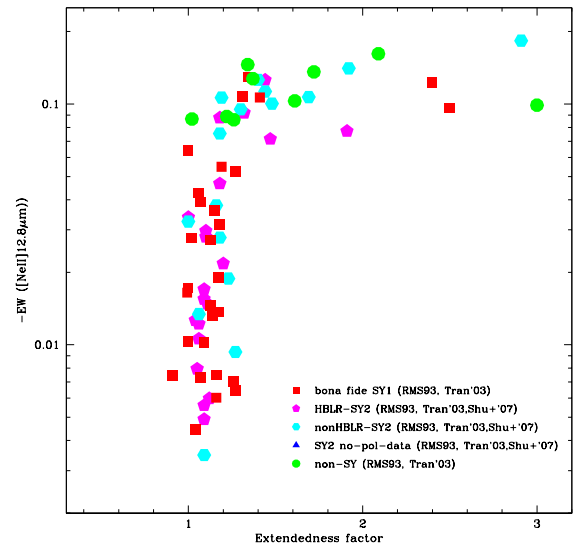


Fig. 19. $[\text{NeII}]12.8\mu\text{m}$ line equivalent width as a function of the source extendedness (Tommasin et al 2008).

The two channels of the *Spitzer* high-resolution spectrometer: SH $9.6-19.5\mu\text{m}$ with slit size $4.7'' \times 11.3''$ and LH $19-39\mu\text{m}$ with slit size $11.1'' \times 22.3''$

allow multi-aperture photometry in the overlapping parts ($19.0\text{-}19.5\mu\text{m}$). The ratio of the flux measured in LH to that measured in SH gives the extendedness of the source. We used this measure of the extendedness of the source to estimate the line emitting regions (Tommasin et al 2008). In Figure 19 we plot the $[\text{NeII}]12.8\mu\text{m}$ line equivalent width as a function of the source extendedness. We notice that those sources showing a significant mid-IR extendedness are type 2 objects or non-Seyfert galaxies and have the highest $[\text{NeII}]12.8\mu\text{m}$ line equivalent width. A high $[\text{NeII}]12.8\mu\text{m}$ line equivalent width is a measure of a strong star formation component. This is not the case for the high excitation lines, originated from the AGN, such as $[\text{NeV}]$ and $[\text{OIV}]$, for which no apparent trend appears between source extendedness and line EWs (Tommasin et al 2008).

5. ANALYSIS OF THE $12\mu\text{m}$ SAMPLE MULTI-FREQUENCY DATASET

The 12MGS has been observed extensively from the radio to the X-rays and we can use the large set of data to search for correlations between different observed quantities. To show an example, we want to relate the X-ray luminosity, measuring the accretion, to the bolometric luminosity, as given by the $12\mu\text{m}$ luminosity. We plot in Figure 20 the *unabsorbed* 2-10keV luminosity and the $12\mu\text{m}$ luminosity.

Following the finding of Spinoglio & Malkan (1989) and Spinoglio et al (1995) that the $12\mu\text{m}$ luminosity is linearly proportional to the *bolometric* luminosity, at a given L_{bol} in Figure 20 a sequence can be identified with decreasing accretion luminosity: from Seyfert 1's \rightarrow HBLR-Seyfert 2's \rightarrow *pure* Seyfert 2's. Although these results are to be considered preliminary, as no statistical method has yet been applied, most Seyfert 1's have:

$$0.1 \times L(12\mu\text{m}) < L(2-10\text{keV}) < L(12\mu\text{m})$$

Most HBLR-Seyfert 2's have:

$$0.01 \times L(12\mu\text{m}) < L(2-10\text{keV}) < 0.1 \times L(12\mu\text{m})$$

Most pure Seyfert 2's and non-Seyfert's have:

$$L(2-10\text{keV}) < 0.01 \times L(12\mu\text{m})$$

We preliminarily suggest that black hole accretion, as measured by X-rays, is the dominant mechanism determining the observational nature of a galaxy: when accretion is not an important energy source, we have galaxies without Seyfert nuclei, dominated by stellar evolution processes (called here non-Seyfert's), then when accretion increases we have a sequence from the *pure* Seyfert 2's, to the HBLR-Seyfert 2's and finally when accretion dominates the bolometric luminosity, we have the Seyfert 1's.

In an analogous way, we try to correlate the IRAS $60\mu\text{m}$ luminosity (measuring the integrated star for-

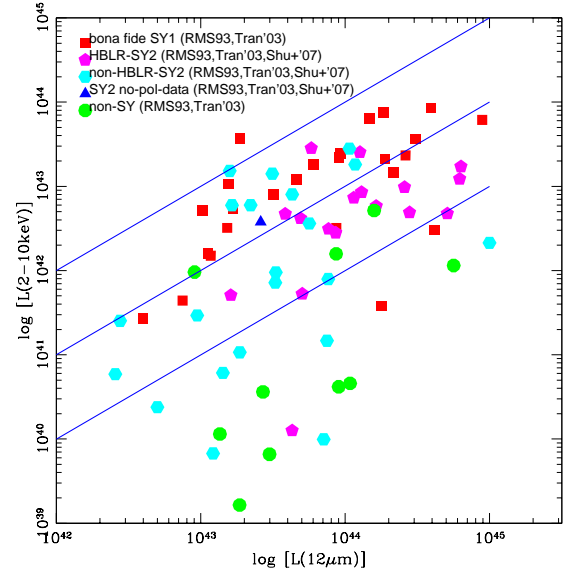


Fig. 20. Corrected (unabsorbed) X-ray (2-10 keV) luminosity as a function of the $12\mu\text{m}$ luminosity. The three lines from the top to the bottom indicate the loci of $L(2-10\text{keV}) = L(12\mu\text{m})$ (*upper*); $L(2-10\text{keV}) = 0.1 \times L(12\mu\text{m})$ (*middle*); and $L(2-10\text{keV}) = 0.01 \times L(12\mu\text{m})$ (*lower*), which are used in the text to roughly separate the different objects.

mation activity) and the H_2 S(1) line luminosity

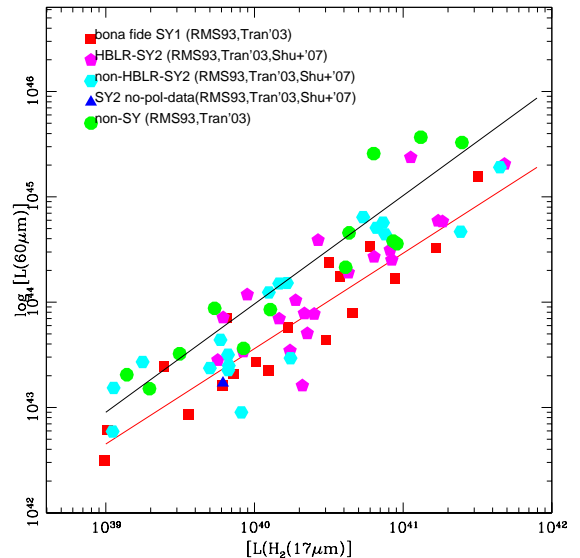


Fig. 21. Total $60\mu\text{m}$ luminosity as a function of the H_2 $17\mu\text{m}$ line luminosity. The two lines from the top to the bottom are least squares fits of the non-Seyfert galaxies and of the Seyfert 1's, respectively (see the text)

(typical star formation indicator) in Figure 21.

Most Seyfert 1's and HBLR-Seyfert 2's have:

$$L(H_2) \sim 5 \times 10^{-4} \times L(60\mu m)$$

Most pure Seyfert 2's and non-Seyfert have:

$$L(H_2) \sim 10^{-4} \times L(60\mu m)$$

If we make least squares fits to the two extreme populations of Seyfert type 1's and non-Seyfert galaxies, we obtain a sequence of two almost parallel lines of the form $\text{Log}(L(60\mu m)) = a \times \text{log}(L(H_2)) + b$ from the bottom to the top:

- for Seyfert 1's: $a=0.905$, $b=7.325$, with a regression coefficient of $R=0.928$;
- for non-Seyfert's: $a=1.030$, $b=2.797$, with $R=0.925$.

There are two interpretations of this behavior: either the more active galaxies (type 1's) have enhanced H_2 emission (Rigopoulou et al 2002), or at a given H_2 luminosity, type 2's (and non-Sy) have $L(60\mu m)$ 5 times higher than type 1's, because of an enhanced star formation process.

6. SPECTROSCOPY OF HIGHER REDSHIFT GALAXIES WITH HERSCHEL & SPICA

To understand how the two processes of black hole accretion and star formation shared the energy budget during galaxy evolution, we need to separate these two processes along the history of galaxies, and -to do this- rest-frame near-to-mid infrared spectroscopy is needed on galaxies as a function of their redshift. We predicted the line intensities of Seyfert and starburst galaxies at increasing redshift, considering the ISO spectra of three local template objects: NGC1068 (Alexander et al 2000; Spinoglio et al 2005), the prototypical Seyfert 2 galaxy, containing both an AGN and a starburst; NGC6240 (Lutz et al 2003), a bright starburst with obscured AGN and M82 (Forster Schreiber et al 2001; Colbert et al 1999), the prototypical starburst galaxy. We then computed the line intensities as a function of redshift (in the range $z=0.1-5$), assuming that the line luminosities scale as the bolometric luminosity and that there is a luminosity evolution proportional to the $(z+1)^2$, consistent with the Spitzer results at least up to redshift $z=2$ (Perez-Gonzalez et al 2005).

For simplicity³, we adopted an Einstein-De Sitter model Universe, with $\Omega_\Lambda = \Omega_{vac} = 0$ and $\Omega_M = 1$,

³ We note that the dependence on different cosmological models is not very strong. The popular model with $\Omega_M = 0.27$, $\Omega_{vac} = 0.73$, $H_0 = 71 \text{ km s}^{-1} \text{ Mpc}^{-1}$ shows greater dilutions, increasing with z , by factors of 1.5 for $z=0.5$ to 2.5 for $z=5$. In this case the line intensities of Figure 22 would decrease by these factors.

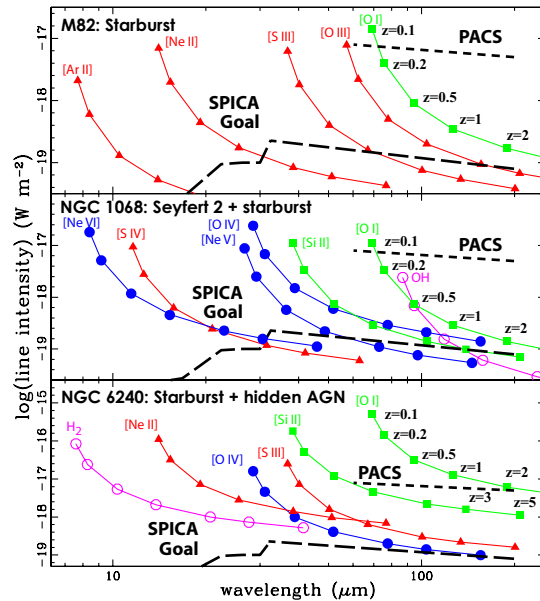


Fig. 22. Line observability with PACS onboard of *Herschel* and with *SPICA*. Few selected diagnostic lines are shown as a function of redshift for the three template objects M82, NGC1068 and NGC6240 (from the top to the bottom). The lines have the same symbols as in Figure 14, except for the open circles, representing molecular lines. Line intensities are given in W m^{-2} . The short dashed and long-dashed lines give the 5σ , 1 hour sensitivities of the PACS and SPICA spectrometers.

$H_0 = 75 \text{ km s}^{-1} \text{ Mpc}^{-1}$. The luminosity distances have been derived using:

$$d_L(z) = (2c/H_0) \cdot [1 + z - (1 + z)^{1/2}]$$

The results for the three template objects are reported in a graphical form in Figure 22, where the intensities of selected lines are plotted as a function of the redshift. Among the brightest lines are shown the [SIV]10.5 μm , the [NeII]12.8 μm and the [OIII]52 μm diagnostic for the stellar/HII regions; the [NeV]24.3 μm and the [OIV]25.9 μm , for the AGN component, the [OI]63 μm and the [SiII]33.5 μm , for the photodissociation regions and the OH and H_2 rotational lines for the warm molecular component.

The 5σ , 1 hour sensitivities of the PACS spectrometer onboard of *Herschel* and of the two spectrometers foreseen at the focal plane of the JAXA mission *SPICA* (Space Infrared Telescope for Cosmology and Astrophysics) (Nakagawa 2004; Swinyard et al 2008) are shown in the figure for comparison.

It is clear from the figure that the PACS spectrometer will be able to observe only the most favor-

able object (NGC6240) up to $z=2$ in the brightest line ([OI]63 μ m), while the SPICA spectrometers *goal* sensitivities will allow deep infrared spectroscopic studies for all templates at $z \sim 1-2$ for most lines and at z even higher for the brightest lines.

Acknowledgements: This work has been funded in Italy by the Italian Space Agency (ASI).

REFERENCES

- [Alexander, T. et al 2000, ApJ, 536, 710
 [Bertoldi, F., Carilli, C., Cox, P., et al 2003, A&A, 406, L55
 [Buchanan, C. et al 2006, AJ, 132, 401
 [Colbert et al 1999, ApJ, 511, 721
 [Dopita, M.A., Fischera, J., & Sutherland, R.S. et al. 2006, ApJS, 167, 177
 [Edelson, R.A., Malkan, M.A., Rieke, G.H., 1987, ApJ, 321, 233
 [Fischer, J. et al. 1999, Ap&SS, 266, 91
 [Forster Schreiber et al 2001, ApJ, 552, 544
 [Genzel, R. et al, 1998, ApJ, 498, 579
 [González-Alfonso, E., et al 2004, ApJ, 613, 247
 [González-Alfonso, E., et al 2008, ApJ, 675, 303
 [González Delgado, R., Heckman, T., & Leitherer, C. 2001, ApJ, 546, 845
 [Gorjian, V. et al. 2004, ApJ, 605, 156
 [Groves, B.A., Dopita, M. A., & Sutherland, R.S. 2004, ApJS, 153, 9
 [Hailine, K., Malkan, M.A., Spinoglio, L. & Tommasin, S. 2009, in preparation
 [Heckman, T.M., Kauffmann, G., Brinchmann, J., et al 2004, ApJ, 613, 109
 [Hunt, L.K., & Malkan, M.A. 1999, ApJ, 516, 660
 [Hunt, L.K. et al 1999, ApJ, 510, 637
 [Kauffmann, G., Heckman, T.M., Tremonti, C. et al 2003, MNRAS, 346, 1055
 [Kessler, M. et al 1996, A&A, 315, L27
 [Krongold, Y., Dultzin-Hacyan, D., & Marziani, P. 2002, ApJ, 572, 169
 [Lutz, D. et al 2003, A&A, 409, 867
 [Imanishi, M. 2003, ApJ, 599, 918
 [Imanishi, M. & Alonso-Herrero, A. 2004, ApJ, 614, 122
 [Levenson, N.A., Weaver, K.A., & Heckman, T.M. 2001, ApJ, 550, 230
 [Maiolino, R. Ruiz, M., Rieke, G.H., Keller, L.D. 1995, ApJ, 466, 561
 [Marconi, A., Risaliti, G., Gilli, R., et al 2004, MNRAS, 351, 169
 [Meijerink et al. 2007, A&A, 461, 793
 [Merloni, A., Rudnick, G., & Di Matteo, T. 2004, MNRAS, 354, 37
 [Nakagawa, T. 2004, Advances in Space Research, 34, 645
 [Negishi T. et al. 2001, A&A, 375, 566
 [Perez-Gonzalez, P.G. et al 2005, ApJ, 630, 82
 [Pier E.A. & Krolik, J.H. 1993, ApJ, 418, 673
 [Priddey, R.S., Isaak, K.G., McMahon, R.G., Robson, E.I., & Pearson, C.P. 2003, MNRAS, 344, L74
 [Puget, J.-L. & Leger, A. 1989, ARA&A, 27, 161
 [Raimann, D., Storchi-Bergmann, T., González Delgado, R. M., Cid Fernandes, R., Heckman, T., Leitherer, C., & Schmitt, H. 2003, MNRAS, 339, 772
 [Rigopoulou, D., Kunze, D., Lutz, D., Genzel, R., & Moorwood, A.F.M. 2002, A&A, 389, 374
 [Rodríguez, D. R., Malkan, M. A., Jensen, L., Spinoglio, L., Rush, B. 2008, in preparation
 [Rowan-Robinson, M., & Crawford, J. 1989, MNRAS, 238, 523
 [Rush, B., Malkan, M.A., & Spinoglio, L. 1993, ApJS, 89, 1 (RMS).
 [Rush, B., Malkan, M.A.; Fink, H.H., Voges, W. 1996, ApJ, 471, 190
 [Rush, B., Malkan, M.A., Edelson, R. A., 1996, ApJ, 473, 130
 [Schmitt, H., Storchi-Bergmann, T., & Cid Fernandes, R. 1999, MNRAS, 303, 173
 [Shu, X. W. et al 2007, ApJ, 657,167
 [Spinoglio, L. & Malkan, M.A. 1989, ApJ, 342, 83
 [Spinoglio, L. & Malkan, M.A. 1992, ApJ, 399, 504 (SM92)
 [Spinoglio, L., Malkan, M.A., Rush, B., Carrasco, L., Recillas-Cruz, E. 1995, ApJ, 453, 616
 [Spinoglio, L., Andreani, P., Malkan, M.A. 2002, ApJ, 572, 105
 [Spinoglio L., Malkan, M. A., Smith, H. A., et al. 2003, *Active Galactic Nuclei: from Central Engine to Host Galaxy*, Meudon, France, July 23-27, 2002, Eds.: S. Collin, F. Combes and I. Shlosman. ASP (Astronomical Society of the Pacific), Conference Series, Vol. 290, p. 557
 [Spinoglio, L., Malkan, M.A., Smith, H.A., Gonzalez-Alfonso, E., Fischer, J. 2005, ApJ, 623, 123
 [Storchi-Bergmann, T., et al 2001, ApJ, 559, 147
 [Swinyard, B., Nakagawa, T. et al 2008, Experimental Astronomy, in press
 [Thean, A. et al 2000, MNRAS, 314, 573
 [Thean, A. et al 2001, MNRAS, 325, 737
 [Tommasin, S., Spinoglio, L., Malkan, M.A., Smith, H., Gonzalez-Alfonso, E. & Charmandaris, V. 2008, ApJ, 676, 836.
 [Tommasin, S., Spinoglio, L., Malkan, M.A., Smith, H. 2009, in preparation
 [Tran, H.D., 2001, ApJ, 554, L19
 [Tran, H.D., 2003, ApJ, 583, 632